Langmuir

Article

pubs.acs.org/Langmuir

Superspreaders Versus "Cousin" Non-Superspreaders: Disjoining Pressure in Gravitational Film Drainage

S. Sett,[†] R. P. Sahu,[†] S. Sinha-Ray,[†] and A. L. Yarin*[,†,‡]

[†]Department of Mechanical and Industrial Engineering, University of Illinois at Chicago, 842 West Taylor Street, Chicago Illinois 60607-7022, United States

[‡]College of Engineering, Korea University, Seoul, South Korea

Supporting Information

ABSTRACT: Gravitational drainage of vertical films supported on a wire frame of two superspreaders SILWET L-77 and BREAK-THRU S 278 and their respective "cousin" non-superspreaders SILWET L-7607 and BREAK-THRU S 233 revealed drastic differences. The superspreader films showed complicated dynamic "turbulent"-like interferometric patterns in distinction from the ordered color bands of the "cousin" non-superspreaders, which resembled those of the ordinary surfactants. Nevertheless, the superspreader films stabilized themselves at the thickness about 35 nm and revealed an order of magnitude longer lifetime before bursting compared to that of the "cousin" non-superspreaders. Notably, the superspreaders revealed drastic differences from the non-superspreaders in aqueous solutions *with no contact with any solid hydrophobic surface*. The self-stabilization of the superspreader films is attributed to significant disjoining pressure probably related to long superspreader bilayers hanging from the free surfaces. The scaling law for the disjoining pressure was found as $p_{disj}(h) \sim h^{-m}$ (with $m \approx 9-11$) for the sufficiently concentrated superspreader solutions, and as $p_{disj}(h) \sim h^{-s}$ (with $s \approx 6$) for more dilute solutions (in both cases, concentrations were above the critical micelle concentration). The non-superspreaders do not possess any significant disjoining pressure even in the films with thicknesses in the 35−100 nm range. The results show that gravitational drainage of vertical films is a useful simple tool for measuring disjoining pressure.

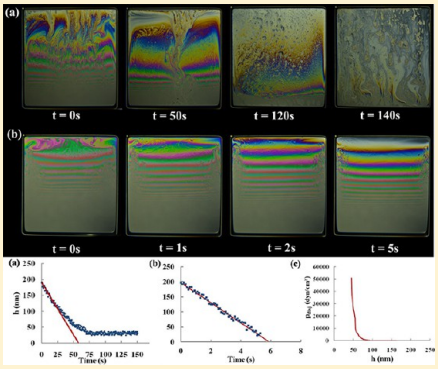

INTRODUCTION

The aqueous solutions of trisiloxane-(poly)ethoxylate surfactants are widely applied as agricultural adjuvants, solid modifiers, and cleaners. Such surfactants are commonly denoted as M(D′E_nOMe)M, with M-D′-M being the trisiloxane hydrophobe, E_n - the ethylene oxide, Me - the methyl group, and O - oxygen.[1] Water drops with added superspreaders easily spread on hydrophobic surfaces such as polyethylene (PE) or polypropylene (PP). The superspreading ability of trisiloxane-(poly)ethoxylate surfactants is determined by the length of the (poly)ethylene oxide group. Two drastically different "cousin" types of trisiloxane-(poly)ethoxylate surfactants with n = 7.5 (which is the superspreader known under the product name SILWET L-77; ref 1) and n = 16 [which is the non-superspreader, denoted as M(D′E_n)M under the product name SILWET L-7607, ref 2] are distinguished. The superspreader BREAK-THRU S 278 has a similar nominal structure as that of SILWET L-77 (ref 3). Its "cousin" non-superspreader BREAK-THRU S 233 has an OH-terminated polyether group containing both ethylene oxide and propylene oxide.[3] The length of the poly(ethylene oxide) increases, thereby indicating a larger hydrophilic headgroup for the non-superspreaders SILWET L-7607 and BREAK-THRU S 233 than that of the superspreaders SILWET L-77 and BREAK-THRU S 278, respectively.

The physicochemical origins of the superspreading on hydrophobic surfaces are debated.[1−3] Formation of bilayer structures was assumed for superspreaders and argued to be the reason of the superspreading effect on hydrophobic surfaces.[1] On the other hand, the "cousin" non-superspreaders presumably do not form large-scale bilayer structures above the critical micelle concentration (cmc) but rather ordinary micelles.[1] Superspreading is frequently related to the assumed propensity of superspreaders to settle onto hydrophobic substrates close to the moving contact line, which presumably leads to an increase in surface tension there, the increased concentration-gradient-related Marangoni effect, and an enhanced spreading.[4,5]

In the present work, gravitational drainage of vertical films of the aqueous solutions of the above-mentioned superspreaders and their "cousin" non-superspreaders is studied using the setup similar to the one described in our recent work.[6] Even though superspreader solutions do not contact with any hydrophobic solid surfaces in the present case of gravitational drainage, their behavior is radically different from that of the "cousin" non-superspreaders and the ordinary surfactants. Namely, a dramatic deceleration of the drainage process at the later stage is observed,

Received: August 15, 2013
Revised: February 12, 2014

   dx.doi.org/10.1021/la404754d | *Langmuir* XXXX, XXX, XXX−XXX

which makes superspreader films much more stable than their non-superspreader counterparts. The reason of the unusual behavior of superspreaders in the case of gravitational drainage is traced to their disjoining pressure. Disjoining pressure is associated with the internal energy-related part of the free energy, in distinction from the osmotic pressure, which is associated with the entropy-related part of the free energy.[7] The disjoining pressure strongly depends on the film thickness h when $h < 100$ nm, and the dependence (the scaling or the oscillatory character) is determined by the intersurface repulsion mechanisms in the film on the microscopic level.[7−10] For example, the electrostatic repulsion in the DLVO theory, the van der Waals attraction and repulsion, as well as the steric repulsion and micelle ordering, result in drastically different dependences of the disjoining pressure on the film thickness h.[7−12]

Disjoining pressure was measured using Scheludko[13,14] and/or Mysels-Jones[10,15] cells for many ordinary cationic, anionic, and nonionic surfactants. In the present work we introduce an alternative technique, gravitational film drainage, and apply it to superspreaders and their "cousin" non-superspreaders. The following section describes the materials and the experimental setup and method. Then, the experimental results are presented. After that, the theoretical section is given, which is followed by the comparison with the experimental data and discussion. Conclusions are drawn at the end.

EXPERIMENTAL SECTION

Materials. The following trisiloxane-(poly)ethoxylate surfactants were used in drainage experiments. SILWET L-77 (superspreader) and SILWET L-7607 (the "cousin" non-superspreader), both obtained from Momentive, were used as received. In addition, BREAK-THRU S 278 (superspreader) and BREAK-THRU S 233 (the "cousin" non-superspreader), obtained from Evonik Industries were used as received.

Solution Preparation. Trisiloxane surfactants SILWET L-77, SILWET L-7607, BREAK-THRU S 278, and BREAK-THRU S 233 were used to prepare solutions as follows. Using the superspreader SILWET L-77, 0.1, 0.2, 0.5, and 1 mL of the surfactant was added to 100 mL of deionized water (ASTM Type II). The resulting solutions were denoted as L-77-0.1, L-77-0.2, L-77-0.5, and L-77-1.0, respectively. Using the "cousin" non-superspreader SILWET L-7607, 0.1, 0.2, 0.5 and 1 mL of the surfactant was added to 100 mL of deionized water (ASTM Type II), and the resulting solutions were denoted as L-7607-0.1, L-7607-0.2, L-7607-0.5, and L-7607-1.0, respectively. Using the superspreader BREAK-THRU S 278 and the "cousin" non-superspreader BREAK-THRU S 233, solutions were prepared similarly. The BREAK-THRU S 278 solutions were denoted as S 278-0.1, S 278-0.2, S 278-0.5, and S 278-1.0. The BREAK-THRU S 233 solutions were denoted as S 233-0.1, S 233-0.2, S 233-0.5, and S 233-1.0.

Experimental Setup and Method. The experimental setup and method used to study drainage of vertical plane surfactant films is described elsewhere.[6] In brief, Figure 1 depicts the schematic which shows how the container with a surfactant solution is raised using the linear actuator to create a film supported by the fixed aluminum wire frame (4 cm ×4 cm x 0.087 cm). The container is then lowered, and the film that stays on the frame is photographed using a CCD camera (Phantom Miro 4), while the data are stored in the computer. It was found that fully reliable and self-consistent data can be acquired for film thicknesses above 30 nm.[6]

The film thickness at the top was measured right below the top wire and 2 cm from the left wire, so the side wires did not have any effect on the film thickness. The local film thickness h was calculated using the interferometric formula.[6,16−20]

EXPERIMENTAL RESULTS

The cmc of each of the four surfactants was determined by measuring the surface tension using the Wilhelmy plate

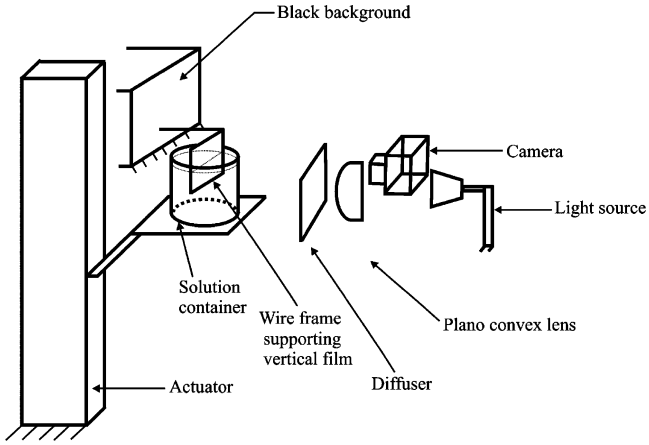

Figure 1. Schematic of the experimental setup.

apparatus (KRUSS Tensiometer K 12)[21,22] with the plate dimensions of 20 mm × 10 mm. The data in Figure S1 of the Supporting Information (SI) show that at the concentration 0.007 %v/v, for SILWET L-77, SILWET L-7607, BREAK-THRU S 278 and BREAK-THRU S 233 the surface tensions had saturated. This value was considered as the cmc value corresponding to these surfactants. The concentration of all the solutions used in the drainage experiments was above their cmc.

Dynamic light scattering (DLS) was used to measure the aggregate sizes formed in solutions of SILWET L-77, SILWET L-7607, BREAK-THRU S 278, and BREAK-THRU S 233 at concentration 0.5 %v/v above the cmc. The solutions prepared from the superspreaders SILWET L-77 and BREAK-THRU S 278 were turbid in appearance, and the turbidity was found to increase with concentration. It is evident from Figure 2 that the superspreader solutions contain aggregates which are 2 orders of magnitude larger than their counterpart non-superspreaders. The aggregate structures in the superspreader solutions combine and form larger entities (Figure 2a,c) known as mesomorphic phases.[23] These are anisotropic structures causing solution turbidity and resulting in light scattering. Increasing surfactant concentration increases the number of such aggregates, and thus, turbidity. On the contrary, solutions prepared from the "cousin" non-superspreaders SILWET L-7607 and BREAK-THRU S 233 stayed clear. They formed smaller aggregates/micelles (Figure 2b,d) that are too small to cause any significant light scattering.[23]

The size of aggregates formed in surfactant solutions depends on the critical packing parameter P[8,24]

$$P = \frac{V}{a_0 l_c} \tag{1}$$

where V is the chain volume, a_0 is the optimal aggregate−water interfacial area (the hydrocarbon/water interfacial area), and l_c is the critical chain length.

For surfactants with the hydrophilic headgroup larger than the hydrophobic part ($P < 1$), curved aggregates such as spherical or cylindrical micelles are formed. For comparable sizes of hydrophilic and hydrophobic parts, $P = 1$, surfactant bilayer aggregates are formed.[8,24] For trisiloxane surfactants, the length of poly(ethylene oxide) increases from 7.5 for SILWET L-77 to 16 for SILWET L-7607. A similar increase in the length of poly(ethylene oxide) is found when BREAK-THRU S 278 and BREAK-THRU S 233 are compared. The small hydrophilic headgroup in the superspreaders SILWET L-77 and

dx.doi.org/10.1021/la404754d | Langmuir XXXX, XXX, XXX−XXX

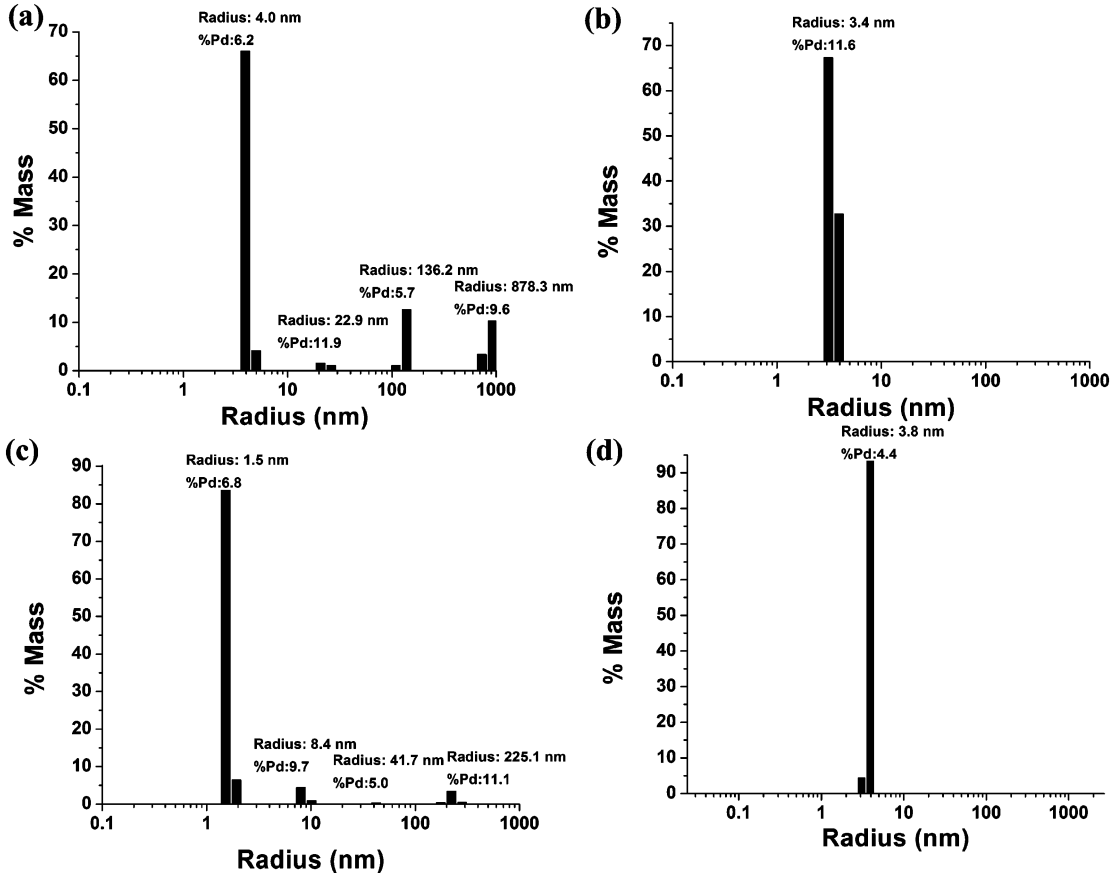

Figure 2. Aggregate size distribution for 0.5 %v/v solutions of (a) SILWET L-77, (b) SILWET L-7607, (c) BREAK-THRU S 278, and (d) BREAK-THRU S 233. %Pd stands for the percentage of polydispersity which is a measure of standard deviation and is indicative of the distribution of each peak. %Mass is the percentage of mass of aggregates of a particular size present in the solution.

BREAK-THRU S 278 results in formation of larger aggregates (vesicles and bilayers) and turbid solutions as compared to the smaller micellar aggregates of the non-superspreaders SILWET L-7607 and BREAK-THRU S 233, and their clear solutions. This is in agreement with a well-established fact that surfactants having shorter hydrophilic chains form large aggregates, while those with longer chains form smaller aggregates.[1,25]

Solutions with different concentrations of the superspreaders SILWET L-77 and BREAK-THRU S 278, and their non-superspreader counterparts SILWET L-7607 and BREAK-THRU S 233, respectively, were used in the gravitational drainage experiments. For SILWET L-77 solution L-77-0.1, it was observed that initially the interference color bands were formed. These color bands were not uniform horizontally, and each color strip was of uneven thickness. With time, the visible colors in the upper part of the wire frame mixed with one another, indicating nonuniform film thickness in the horizontal direction. Toward the bottom of the wire frame, the film became turbid with time, and no distinct colors could be seen in a while. After 55 s from the formation of the film, the topmost part of the film turned black, where the measured thickness was ∼50 nm (Figure 3a). The top part of the film remained black for the remaining time. The black domain was confined to the topmost part and did not spread downward with time. The color intermittency over the entire film further increased gradually till the film burst after 105 s (Figure 3a, the inset image). It is emphasized that the "abstract" color patterns in all the superspreader solutions as shown in Figure 3 (the inset images) are dramatically different from the regular horizontal color bands observed before for the ordinary cationic, anionic and nonionic surfactants.[6] As it is shown below, the "abstract" color patterns of the superspreader solutions are also very different from those of the cousin non-superspreaders.

For SILWET L-77 solution L-77-0.2, similar observations were done. The black film had been formed at the film top after 65 s (Figure 3b). It descended down with time and a considerable part of the film at the top was black when the film burst after 118 s (Figure 3b, the inset image). For SILWET L-77 solution L-77-0.5, after the initial color intermittency led to an uneven color distribution, plumes were seen to rise from the bottom, indicating that the thickness distribution is uneven and highly transient. The plumes made the bottom part of the film blurred and no distinct colors were seen in these regions. The top part of the film turned black after 72 s (Figure 3c) and the black domain advanced downward with time. The black film occupied at about one-half of the film length along the wire frame at the time of bursting after 150 s (Figure 3c, the inset image).

It should be emphasized that the color intermittency in the horizontal direction over the superspreader films in Figure 3 according to the interferometric formula[6,21−25] corresponds to the film thickness variation in the horizontal direction Δh on the scale of $\Delta h = \Delta\lambda/(2\pi n)$, with $\Delta\lambda$ being the wavelength difference between the two colors, and n being the refractive index (n = 1.333). In the worst case of red color replaced by blue color or vice versa, $\Delta h \approx 23.8$ nm, which would result in variance close to ±10 nm about the mean. In reality, the color intermittency is less than in the worst case, and the results shown in Figure 3 reveal the following accuracies corresponding to the thinnest films

dx.doi.org/10.1021/la404754d | *Langmuir* XXXX, XXX, XXX−XXX

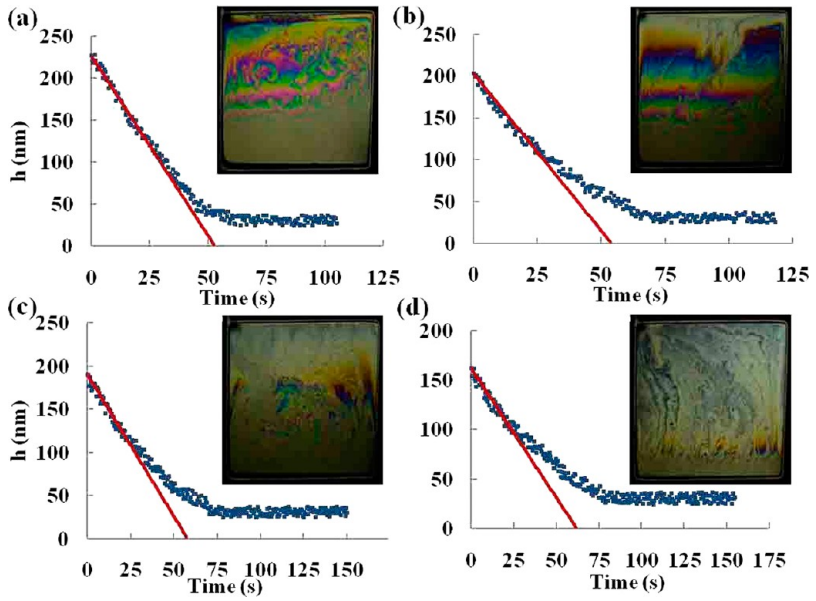

Figure 3. Drainage of the plane films of the superspreader SILWET L-77 solutions: (a) L-77-0.1, (b) L-77-0.2, (c) L-77-0.5, and (d) L-77-1.0. The data correspond to the film top. The experimental results are shown by symbols. The inclined straight lines correspond to the theoretical prediction of ref 6, eq 16 in the present work. The inset images show the interference patterns just prior to the film bursting.

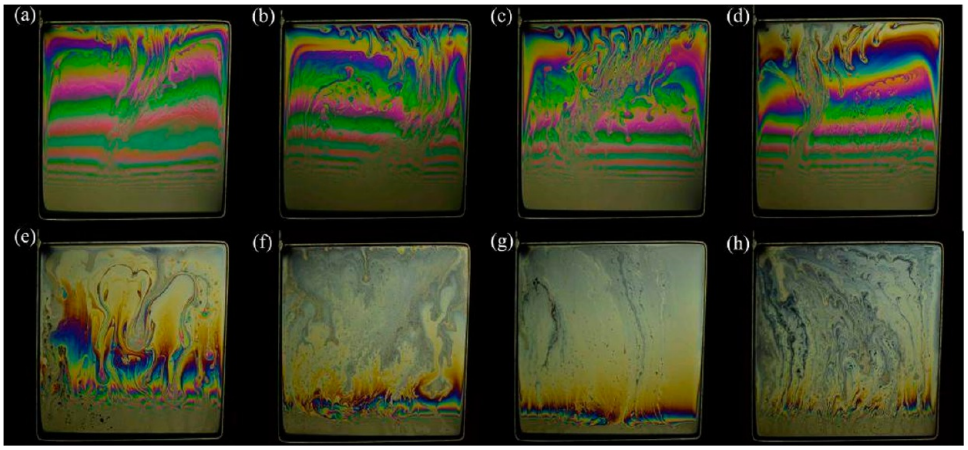

Figure 4. Drainage of the superspreader SILWET L-77−1.0 film at: (a) $t = 0$ s, (b) $t = 25$ s, (c) $t = 50$ s, (d) $t = 70$ s, (e) $t = 90$ s, (f) $t = 110$ s, (g) $t = 130$ s, and (h) $t = 155$ s.

stabilized by the superspreader: Figure 3a: 36 ± 4 nm (L-77-0.1), Figure 3b: 35 ± 3 nm (L-77-0.2), Figure 3c: 36 ± 3 nm (L-77-0.5), and Figure 3d: 35 ± 3 nm (L-77-1.0). This shows that the accuracy is sufficient even at the lowest data branches for the highly intermittent films of superspreader solutions. Note also that measurements were done only when distinct colors were fully recognizable, whereas turbid areas near the bottom of the wire frame were never used.

The time evolution of the film of the superspreader SILWET L-77 solution L-77−1.0 is illustrated in Figure 4. In such a film, the number of rising plumes increased and eventually could be seen covering the entire film. "Turbulent"-like patterns seen on the film were also much larger compared to the lower concentration films. The black film formed at the top after 78 s (Figure 3d, the inset image, and Figure 4e), increased with time and covered the entire film at the moment of bursting (Figure 3d, the inset image, and Figure 4h).

Even though the superspreader films looked pretty agitated and transient (Figure 3, the inset images, and Figure 4), they showed a remarkable stabilization at the latter stage of their existence, as is seen in Figure 3. They were stabilized at thicknesses ~35 nm, where they stopped thinning linearly in time,[6] and their thinning was practically arrested for a long time. This is dramatically different from the observations of drainage of the ordinary cationic, anionic and nonionic surfactants (refs 6 and 26 and references therein, and the cousin non-superspreaders discussed below).

For the second superspreader studied in this work, BREAK-THRU S 278, similar trends were observed to those in Figure 3 for the superspreader SILWET L-77. The corresponding results for solutions S 278-0.1 to S 278-1.0 are presented in Figure S2 of the SI. With the increase in the surfactant concentration, the length of the black section at the film top at the time of bursting increases and reaches the maximum for S 278-1.0 (Figure S2, the inset images). Even for BREAK-THRU S 278 solution S 278-1.0 (Figure S2d, the inset image), the black film did not spread over the entire film length, in distinction from the superspreader SILWET L-77 in Figure 3d (the inset image). Also, "plumes"

dx.doi.org/10.1021/la404754d | *Langmuir* XXXX, XXX, XXX−XXX

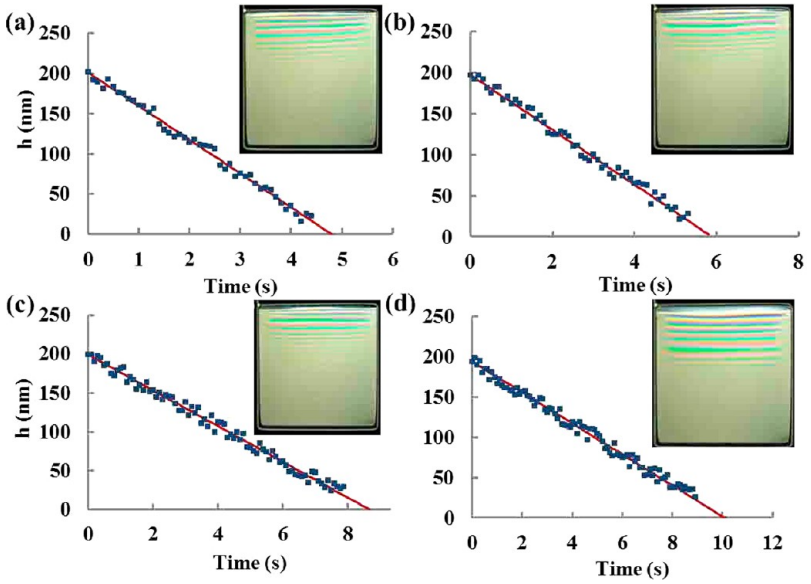

Figure 5. Drainage of the non-superspreader SILWET L-7607 solution films: (a) L-7607-0.1, (b) L-7607-0.2, (c) L-7607-0.5, and (d) L-7607-1.0. The data correspond to the film top. The experimental results are shown by symbols. The films burst in about 5−10 s. The inclined straight lines correspond to the theoretical prediction of ref 6, eq 16 in the present work. The inset images show the interference patterns just prior to the film bursting.

were seen to rise from the bottom of the wire frame for BREAK-THRU S 278 solution S 278-0.2 (Figure S2b, the inset image) and the intensity of these plumes increased for S 278-0.5 (Figure S2c, the inset image) and S 278-1.0 (Figure S2d, the inset image).

Figure 5 shows that the experimental data for the non-superspreader SILWET L-7607 is in good agreement with eq 16 (see the theoretical part below), which reveals a linear decrease in the film thickness during the gravitational drainage near the film top. This is similar to the cationic, anionic, and nonionic surfactants studied earlier,[6,26] and is drastically different from the results for the "cousin" superspreader SILWET L-77 shown in Figure 3.

For the non-superspreader SILWET L-7607 solution L-7607-0.1, the films burst just after the top part turned black (Figure 5a, the inset image). The length of the black film part on top of the film increased only slightly with the increase in the surfactant concentration, in distinction from the "cousin" superspreader SILWET L-77 (cf. Figure 3, the inset images, and Figure 4). In fact, only for SILWET L-7607 solution L-7607-1.0 was there a noticeable increase in the black film length at the time of bursting (Figure 5d, the inset image).

Gravitational drainage of plane vertical films of the non-superspreader BREAK-THRU S 233 solutions S 233-0.1, S 233-0.2, S 233-0.5, and S 233-1.0 revealed a linear decrease in the film thickness (Figure S3 of SI) with no stabilization characteristic of the superspreader counterpart BREAK-THRU S 278 (Figure S2 of SI).

Solutions of the non-superspreader BREAK-THRU S 233 revealed similar regular horizontal interference color strips like those of the non-superspreader SILWET L-7607 solutions (Figure 5, the inset images) or the solutions of the ordinary cationic, anionic, and nonionic surfactants studied in refs 6 and 26 and references therein. On the other hand, such film patterns are drastically different from those for both superspreaders SILWET L-77 (Figure 3, the inset images, and Figure 4) and BREAK-THRU S 278 (Figure S2, the inset images, of the SI). Only the small top parts of the non-superspreader BREAK-THRU S 233 films turned black before the bursting (Figures S3, the inset images).

Overall, the thin films formed from the superspreader solutions were stable for a much longer time in comparison with the cousin non-superspreaders and the ordinary surfactants,[6,26] albeit also much more vigorous (Figures 3, 4, and S2, the inset images, versus Figures 5 and S3, the inset images). The thinning of the superspreader films was practically arrested at the latter stage, whereas the "cousin" non-superspreader films continued to drain (Figures 3 and S2 versus Figures 5 and S3). The thin films formed by the superspreaders (cf. Parts 1 and 2 of the video in the SI, and Figures 6a,c) revealed a "turbulent"-like motion (a pretty stable motion) visibly different from the marginal regeneration,[27−32] which is a destabilizing effect. On the other hand, the non-superspreader films (cf. Parts 3 and 4 of the video in the SI and Figure 6b,d) revealed the ordered drainage pattern characteristic of the ordinary surfactants (refs 6 and 26 and references therein).

THEORETICAL

Effect of Disjoining Pressure on Drainage Rate. Gravitational drainage of a vertical plane film of surfactant solution suspended on a wide rectangular wire frame sketched in Figure 7 was theoretically studied in ref 6 for the cases where the films were sufficiently thick for the disjoining pressure to be neglected. The theory accounts for the surfactant concentration gradient-driven Marangoni flow associated with the surface elasticity and directed upward, which decelerates the gravity-driven drainage. In addition, in the present work, a generalization for the case where the disjoining pressure is important is proposed. The need for such generalization is motivated by the experimental data for the superspreaders, which revealed dramatic stabilization of the drainage process at the latter stages in Figures 4 (for SILWET L-77) and S2 (in the SI, for BREAK-THRU S 278).

In Figure 7 the coordinate reckoned in the drainage direction is denoted as x and the coordinate normal to it as y.

dx.doi.org/10.1021/la404754d | *Langmuir* XXXX, XXX, XXX−XXX

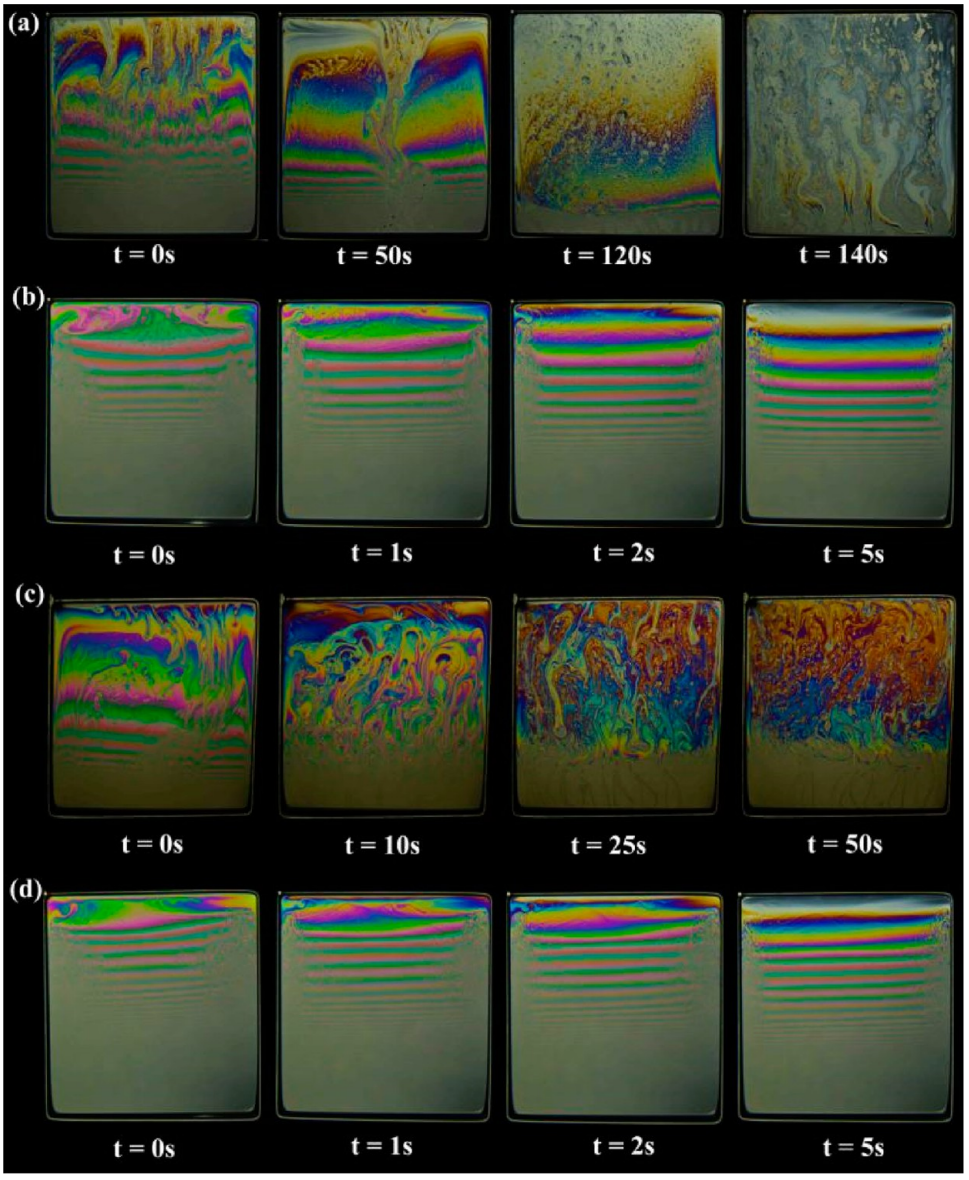

Figure 6. Drainage of (a) the superspreader SILWET L-77, and (b) its "cousin" non-superspreader SILWET L-7607. Drainage of the superspreader (c) BREAK-THRU S 278, and (d) its "cousin" non-superspreader BREAK-THRU S 233.

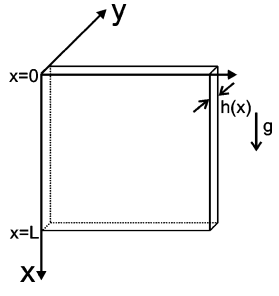

Figure 7. Sketch of a plane vertical surfactant film on a wire frame.

The quasi-one-dimensional mass balance equation for the film drainage[6] can be written as

$$\frac{dh}{dt} = \frac{\partial h}{\partial t} + u\frac{\partial h}{\partial x} = -h\frac{\partial u}{\partial x} \tag{2}$$

with h being the film thickness, u being the longitudinal velocity component, t being time, and dh/dt being the material time derivative.

The normal stresses in viscous liquid in the film read

$$\sigma_{xx} = -p + 2\mu\frac{\partial u}{\partial x}, \quad \sigma_{yy} = -p + 2\mu\frac{\partial v}{\partial y} \tag{3}$$

with p being pressure, v being the transversal velocity component, and μ being the viscosity.

In the quasi-one-dimensional approximation, the stress σ_{yy} is constant across the film, and thus, $\sigma_{yy} = -p_\gamma - p_{disj}$ where p_γ and p_{disj} are the capillary and disjoining pressure. Then, pressure in the film is found as

$$p = p_\gamma + p_{disj} - 2\mu\frac{\partial u}{\partial x} \tag{4}$$

where use is made of the fact that due to the continuity equation $\partial v/\partial y = -\partial u/\partial x$.

dx.doi.org/10.1021/la404754d | *Langmuir* XXXX, XXX, XXX−XXX

Table 1. Superspreader SILWET L-77 Solution Films[a]

solution	t (s)	t_b (s)	x (cm)	$h_i = h_0$ (nm)	T (s)	ε (g/s^2)
L-77-0.1	105	55	0.15	227.03	53	0.176
L-77-0.2	118	65	1.25	202.86	54	0.151
L-77-0.5	150	72	1.95	190.89	58	0.148
L-77-1.0	155	78	3.10	161.15	62	0.124

[a]The film lifetime is denoted t; t_b denotes the time at which black film sets in at the top of the wire frame. The x column corresponds to the position at the film center (reckoned from the top) to which the black film reached at the moment of bursting. The initial film thickness at the top is denoted $h_i = h_0$; the characteristic drainage time is denoted as T. The values of the surface elasticity ε were found from T using eq 17.

Combining the first eq 3 and eq 4 yields

$$\sigma_{xx} = 4\mu\frac{\partial u}{\partial x} - p_\gamma - p_{\mathrm{disj}} \tag{5}$$

and, correspondingly, the total normal force in the film cross-section reads

$$\sigma_{xx}h + 2\gamma = 4\mu h\frac{\partial u}{\partial x} - p_\gamma h - p_{\mathrm{disj}}h + 2\gamma \tag{6}$$

with γ being the surface tension.

In the inertialess approximation the quasi-one-dimensional momentum balance equation reads

$$\frac{\partial \sigma_{xx}\mathrm{h}}{\partial x} + \frac{\partial 2\gamma_0}{\partial x} + 2\sigma_{yx,\mathrm{surf}} + \rho g h = 0 \tag{7}$$

where, γ_0 represents an invariable part of the surface tension (if any) and, as usual,[6,33,34] the variable part of the surface tension associated with the concentration Marangoni effect determines the shear stress acting at the film surface $\sigma_{yx,\mathrm{surf}}$. In addition, ρ denotes the liquid density and g is the gravity acceleration.

In the almost uniform films of low viscosity aqueous surfactant solutions the contribution of the first term on the left in eq 7 is negligibly small,[6,26,33] the capillary pressure is absent, also $\partial\gamma_0/\partial x \equiv 0$, and eq 7 reduces to the following form

$$\sigma_{yx,\mathrm{surf}} = -\frac{\rho g h}{2} + \frac{1}{2}\frac{\partial p_{\mathrm{disj}}h}{\partial x} \tag{8}$$

which generalizes eq 3 of ref 6, or eq 12 of ref 26, or eq 3 of ref 33 on the cases where the disjoining pressure is important. It should be emphasized that the theoretical approach to gravitational drainage of surfactant films developed in refs 6 and 33 fully accounts for the surfactant concentration gradient-driven

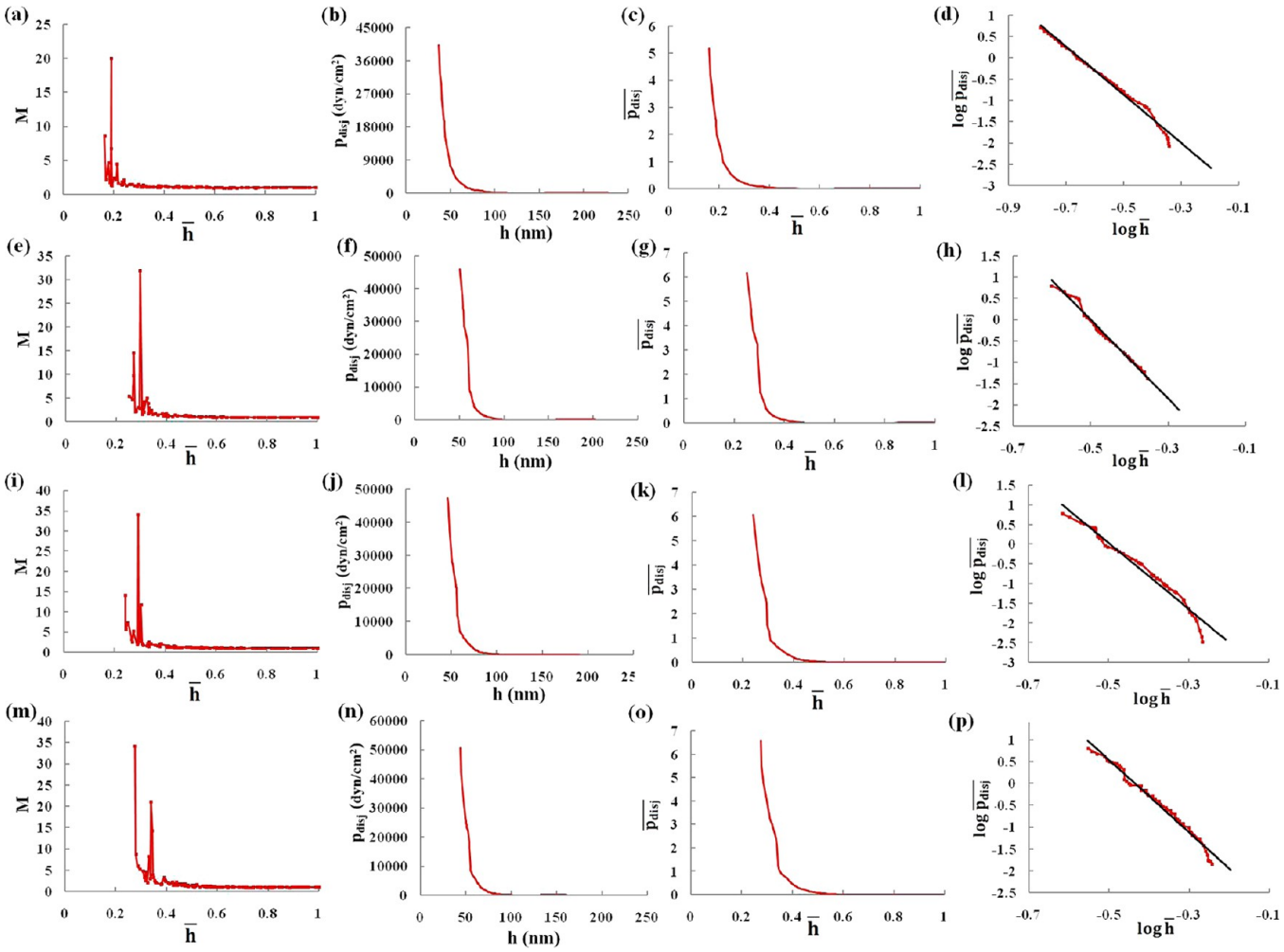

Figure 8. The dependences of M and p_{disj} on the film thickness h for the superspreader SILWET L-77 solutions. L-77-0.1 solution: (a) Function M, (b) the dimensional disjoining pressure, (c) the dimensionless disjoining pressure, (d) scaling of the disjoining pressure: the experimental data is shown in red, the straight line used to determine the exponent in the scaling law is black. The dependences of M and p_{disj} on the film thickness h for the superspreader SILWET L-77-0.2 solution, L-77-0.5 solution, and L-77-1.0 solution are shown similarly in panels e−h, i−l, and m−p, respectively.

dx.doi.org/10.1021/la404754d | Langmuir XXXX, XXX, XXX−XXX

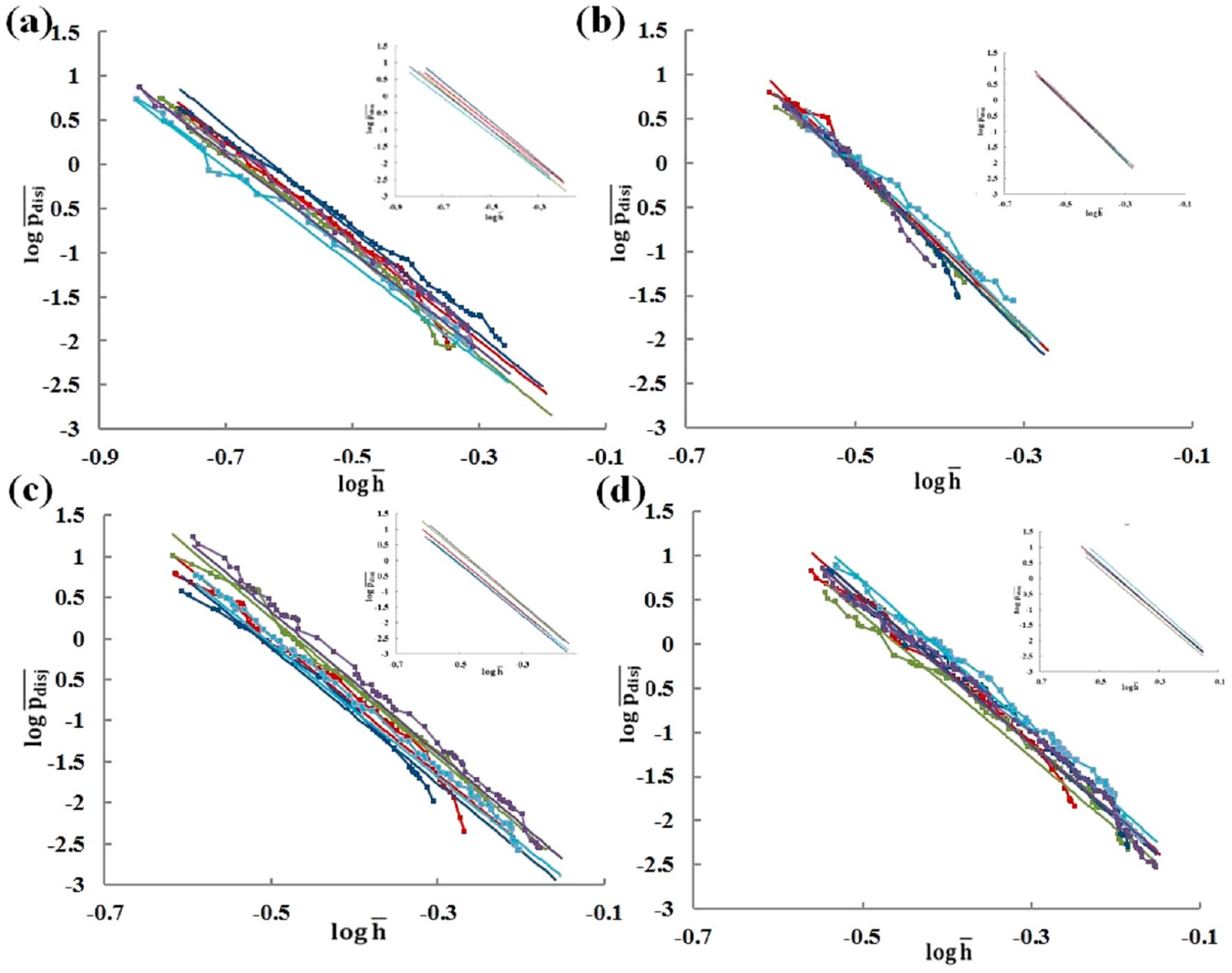

Figure 9. Disjoining pressure versus the film thickness for SILWET L-77 solutions of different concentration: (a) L-77-0.1, (b) L-77-0.2, (c) L-77-0.5, and (d) L-77-1.0. The experimental data is shown with symbols spanned with lines and fitted by continuous straight lines of the corresponding color to determine the exponent in the scaling law. The different colors represent different experimental trials where the initial film thickness varied. The data from Figure 8d,h,l,p is shown in red. The insets show the straight lines corresponding to the scaling laws separately.

Table 2. Scaling Exponents for the Disjoining Pressure of the Superspreader SILWET L-77 Solutions Found Using the Slope of the Scaling Laws Shown in Figure 9a−d

solution	trial 1	trial 2	trial 3	trial 4	trial 5	average exponent
L-77-0.1	−6.38	−6.59	−6.62	−6.15	−6.21	−6.39 ± 0.21
L-77-0.2	−10.7	−10.53	−10.81	−10.95	−10.39	−10.67 ± 0.22
L-77-0.5	−8.66	−8.8	−8.49	−8.37	−8.88	−8.64 ± 0.21
L-77-1.0	−9.37	−9.15	−9.44	−9.56	−9.12	−9.33 ± 0.19

Marangoni effect and the associated surface elasticity of such films.

Taking the material time derivative d/dt of eq 8 and accounting for the relation of $\sigma_{yx,surf}$ with the surface elasticity (the Gibbs elasticity corresponding to the Marangoni effect) $\varepsilon = -\Gamma(\partial\gamma/\partial\Gamma)$, one arrives at the following expression:

$$-\frac{\rho g}{2\varepsilon}\frac{dh}{dt} = \frac{\partial^2 u}{\partial x^2} - \frac{1}{2\varepsilon}\frac{d}{dt}\left(\frac{\partial p_{disj} h}{\partial x}\right) \tag{9}$$

where ε is associated with the dependence of the surface tension γ on the distribution of surfactant concentration Γ at the surface.

Using the mass balance eq 2, we rearrange eq 9 to the following form

$$h = \frac{2\varepsilon}{\rho g}\frac{\frac{\partial^2 u}{\partial x^2}}{\frac{\partial u}{\partial x}} - \frac{1}{\rho g}\frac{\frac{d[\partial(p_{disj} h)/\partial x]}{dt}}{\frac{\partial u}{\partial x}} \tag{10}$$

This equation generalizes eq 9 of ref 6 in the cases where the disjoining pressure is important. Note that

$$\frac{d}{dt}\left(\frac{\partial p_{disj} h}{\partial x}\right) = \frac{d}{dh}\left(\frac{\partial p_{disj} h}{\partial x}\right)\frac{dh}{dt} = \frac{d}{dh}\left(\frac{\partial p_{disj} h}{\partial x}\right)\left(-h\frac{\partial u}{\partial x}\right) \tag{11}$$

dx.doi.org/10.1021/la404754d | Langmuir XXXX, XXX, XXX−XXX

where use was made of eq 2. Then, eq 10 takes the form

$$h = \frac{2\varepsilon}{\rho g}\frac{\frac{\partial^2 u}{\partial x^2}}{\frac{\partial u}{\partial x}}\left[1 - \frac{1}{\rho g}\frac{\mathrm{d}}{\mathrm{d}h}\left(\frac{\partial p_{\mathrm{disj}} h}{\partial x}\right)\right]^{-1} \tag{12}$$

The characteristic length scale along the film is $\varepsilon/(\rho g h)$ [note that it is of the order of 1 cm in the present case]. Using this length scale, the following approximation is made

$$\frac{\mathrm{d}}{\mathrm{d}h}\left(\frac{\partial p_{\mathrm{disj}} h}{\partial x}\right) \approx -\frac{\rho g h}{\varepsilon}\frac{\mathrm{d}p_{\mathrm{disj}} h}{\mathrm{d}h} \tag{13}$$

Table 3. Superspreader BREAK-THRU S 278 Solution Films[a]

solution	t (s)	t_b (s)	x (cm)	$h_i = h_0$ (nm)	T (s)	ε (g/s^2)
S 278-0.1	51	48	0.10	214.21	45	0.137
S 278-0.2	53	50	0.25	202.26	48	0.134
S 278-0.5	61	54	1.00	199.52	51	0.139
S 278-1.0	65	56	2.20	172.26	55	0.121

[a]The film lifetime is denoted t; t_b denotes the time at which black film sets in at the top of the wire frame. The x column corresponds to the position at the film center (reckoned from the top) to which the black film reached at the moment of bursting. The initial film thickness at the top is denoted $h_i = h_0$; the characteristic drainage time is T. The values of the surface elasticity ε were found from T using eq 17.

whereas eq 12 approximately takes the following form:

$$h = \left[\frac{2\varepsilon}{\rho g}\frac{\frac{\partial^2 u}{\partial x^2}}{\frac{\partial u}{\partial x}}\right]\left[1 - \frac{F(h)}{\varepsilon}\right] \tag{14}$$

with

$$F(h) = h\frac{\mathrm{d}}{\mathrm{d}h}[p_{\mathrm{disj}}(h)h] \tag{15}$$

The first multiplier on the right-hand side in eq 14 describes gravitational drainage without accounting for the effect of the disjoining pressure,[6] whereas the second one is the correction associated with the disjoining pressure. Without the effect of the disjoining pressure, the film thickness at the top of the film linearly diminishes in time as

$$h(x, t) = h_0\left(1 - \frac{t}{T}\right) \tag{16}$$

where h_0 is the initial film thickness at the top, and the characteristic time scale T is given by

$$T = \frac{\varepsilon}{\rho(gh_0)^{3/2}} \tag{17}$$

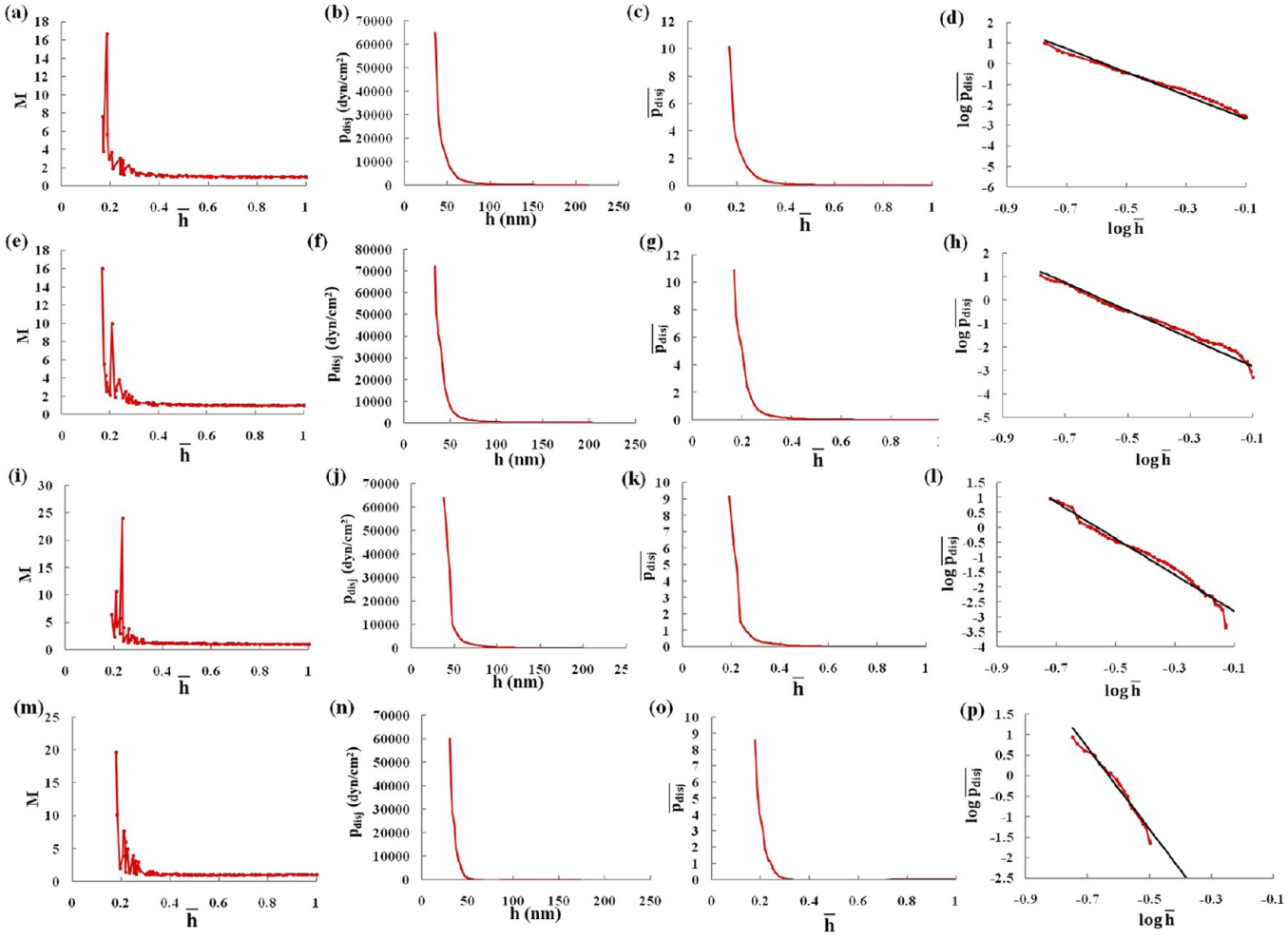

Figure 10. The dependences of M and p_{disj} on the film thickness h for the superspreader BREAK-THRU S 278 solutions. S 278-0.1 solution: (a) Function M, (b) the dimensional disjoining pressure, (c) the dimensionless disjoining pressure, (d) scaling of the disjoining pressure: the experimental data is shown in red, the straight line used to determine the exponent in the scaling law is black. The dependences of M and p_{disj} on the film thickness h for the superspreader BREAK-THRU S 278-0.2 solution, S 278-0.5 solution, and S 278-1.0 solution are shown similarly in panels e–h, i–l, and m–p, respectively.

dx.doi.org/10.1021/la404754d | Langmuir XXXX, XXX, XXX–XXX

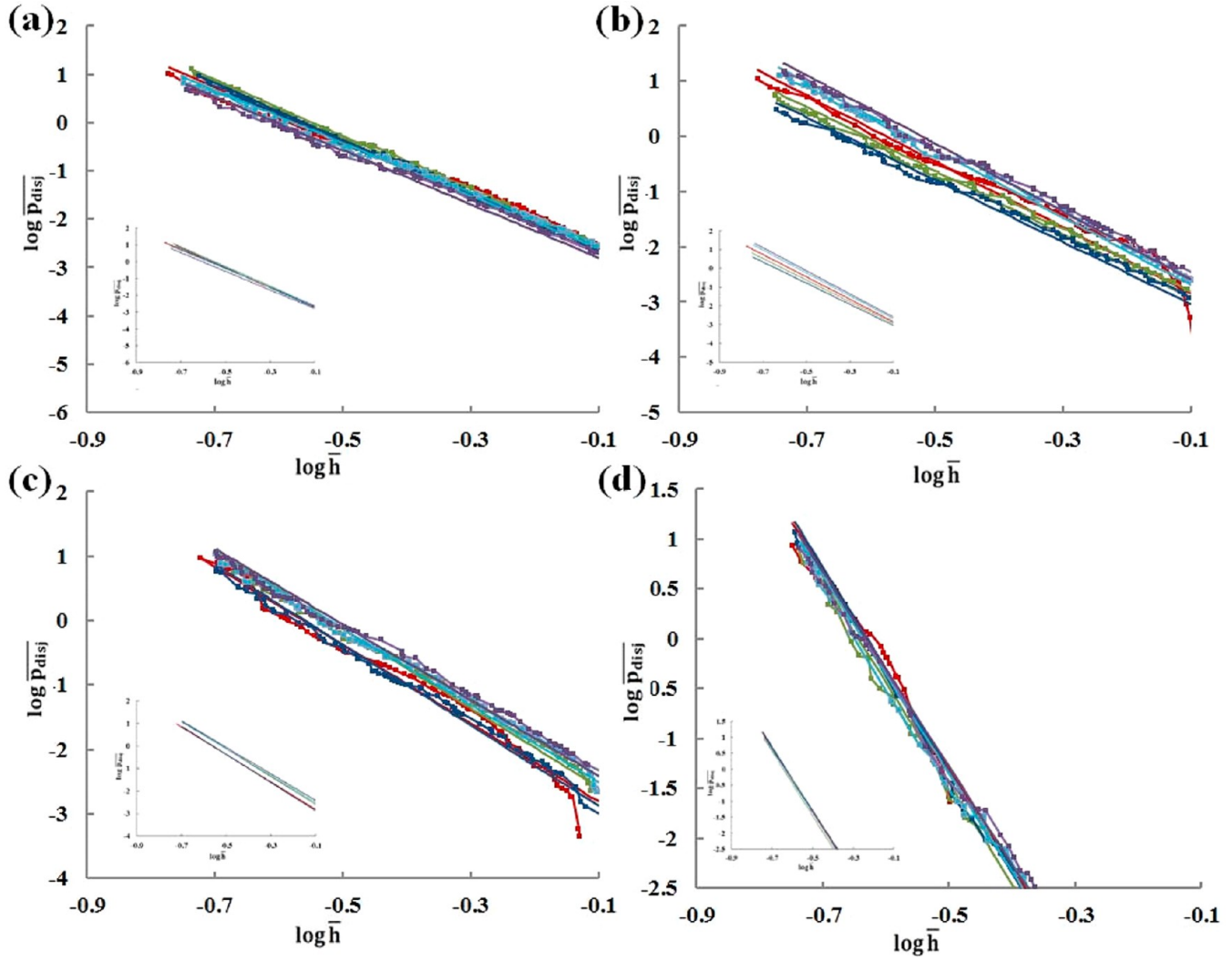

Figure 11. Disjoining pressure versus the film thickness for BREAK-THRU S 278 solutions of different concentration: (a) S 278-0.1, (b) S 278-0.2, (c) S 278-0.5, and (d) S 278-1.0. The experimental data is shown with symbols spanned with lines and fitted by continuous straight lines of the corresponding color to determine the exponent in the scaling law. The different colors represent different experimental trials where the initial film thickness varied. The data from Figure 10d,h,l,p is shown in red. The insets show the straight lines corresponding to the scaling laws separately.

Accounting for the effect of the disjoining pressure, we obtain from eqs 14 and 16 the following expression for the film thickness at the top:

$$\overline{h} = (1 - \overline{t})M(\overline{h}) \tag{18}$$

where the dimensionless film thickness $\overline{h} = h/h_0$, the dimensionless time $\overline{t} = t/T$, and the dimensionless function $M(\overline{h})$ is found using eq 15 as

$$M(\overline{h}) = 1 - \overline{h}\frac{\mathrm{d}}{\mathrm{d}\overline{h}}[\overline{p}_{disj}(\overline{h})\overline{h}] \tag{19}$$

In the latter equation, the disjoining pressure is rendered dimensionless by ε/h_0.

It is emphasized that the function $M(\overline{h})$ can be calculated from the deviation of the experimental data for the film thicknesses of the superspreader solutions from the linear red lines in Figures 3 and S2 (the latter in the SI), i.e., plotting $M(\overline{h}) = \overline{h}/(1 - \overline{t})$ versus $\overline{h}$. Then, the disjoining pressure responsible for the drastic deceleration of the gravitational film drainage is found as

$$\overline{p}_{disj}(\overline{h}) = \frac{1}{\overline{h}}\int_{\overline{h}}^{1}\frac{[M(\overline{h}) - 1]}{\overline{h}}\mathrm{d}\overline{h} \tag{20}$$

which implies that the initial film thickness is large enough to have a negligible disjoining pressure, i.e. $\overline{p}_{disj}(1) = 0$. Note that evaluating the integral in eq 20, we account for the fact that $\overline{h} < 1$.

DISCUSSION: EXPERIMENTS VERSUS THEORY

The data in Figure 3 for the film thickness of the superspreader SILWET L-77 solutions during gravitational drainage was used to find the characteristic time T of the process before the disjoining pressure becomes significant (cf. eqs 16 and 17). Then, using the difference between the measured data and the linear decrease in the film thickness, the function M (cf. eq 18) is established as $M(\overline{h}) = \overline{h}/(1 - \overline{t})$. After that, the disjoining pressure is found from eq 20. The results for the superspreader SILWET L-77 solutions are summarized in Table 1.

The corresponding distributions of M($\overline{h}$) and the disjoining pressure are shown in Figure 8a–p, for the superspreader SILWET L-77-0.1, L-77-0.2, L-77-0.5, and L-77-1.0 solutions, respectively. In addition, the log–log plots of the measured disjoining pressure versus the film thickness for these superspreader solutions are shown in Figure 9a–d to demonstrate the repeatability of the results and evaluate the variance.

dx.doi.org/10.1021/la404754d | *Langmuir* XXXX, XXX, XXX–XXX

Table 4. Scaling Exponents for the Disjoining Pressure of the Superspreader BREAK-THRU S 278 Solutions Found Using the Slope of the Scaling Laws Shown in Figures 11a−d

solution	trial 1	trial 2	trial 3	trial 4	trial 5	average exponent
S 278-0.1	−5.69	−5.85	−5.88	−5.46	−5.55	−5.68 ± 0.18
S 278-0.2	−5.96	−5.75	−5.63	−6.14	−6.11	−5.92 ± 0.22
S 278-0.5	−6.07	−6.14	−6.25	−5.95	−5.88	−6.06 ± 0.15
S 278-1.0	−11.39	−11.56	−11.3	−11.71	−11.25	−11.44 ± 0.19

The scaling exponents found using Figures 9a−d are listed in Table 2.

The data for the superspreader BREAK-THRU S 278 in Figure S2 of the SI was processed similarly to those for the superspreader SILWET L-77. The results for the linear drainage time T and the corresponding surface elasticity ε of BREAK-THRU S 278 are summarized in Table 3.

The distributions of $M(\bar{h})$ and the disjoining pressure found using the data in Figure S2 of the SI are shown in Figures 10a−p for the superspreader solutions BREAK-THRU S 278-0.1, S 278-0.2, S 278-0.5 and S 278-1.0, respectively. In addition, the log−log plots of the measured disjoining pressure versus the film thickness for these superspreader solutions are shown in Figures 11a−11d to demonstrate the repeatability of the results and evaluate the variance. The scaling exponents found using Figures 11a−11d are listed in Table 4.

It is emphasized that the values of the disjoining pressure found in Figures 8 and 10 are in the range up to 6×10^4 dyn/cm^2, which is to be compared to the values up to 15×10^4 dyn/cm^2 measured for the micellar solutions of two nonionic surfactants Brij 35 and Tween 20 using the Scheludko capillary cell or the Mysels−Jones porous-plate cell.[10]

The results in Table 2 show that for the sufficiently concentrated 0.2−1.0 %v/v superspreader SILWET L-77 solutions the measured scaling exponents are close to −9 or −10. On the other hand, for the most dilute solution of 1.0 %v/v, the measured exponent is −6.39 ± 0.21. The results in Table 4 show that for the superspreader BREAK-THRU S 278 only 1.0 %v/v solution revealed the scaling exponent of a high magnitude −11.44 ± 0.19, the other solutions of the superspreader BREAK-THRU S 278 (0.1−0.5 %v/v) revealed the measured exponent close to −6.

The DLS results in Figure 2 imply that in the films formed from the superspreader solutions of sufficient concentration (definitely above the cmc) there are bilayer aggregates of sizes larger than the film thickness h. This can be viewed as the presence of multiple sections of bilayer aggregates hanging from the free surface[1] and forming fluffy surfaces of the film as sketched in Figure 12. Steric repulsions of the entropic origin can certainly decelerate thinning of such films. However, the scaling exponents in Tables 2 and 4 differ from the predictions for any of the entropic steric repulsions, e.g., those discussed in refs 7 and 8. It should be emphasized that in the present case of solutions of nonionic superspreaders in deionized water formation of double layers characteristic of electrolytes is excluded, and thus there is no stabilizing electric forces.

In distinction from the superspreaders, the corresponding non-superspreaders SILWET L-7607 and BREAK-THRU S 233 revealed the linear drainage pattern (Figure 5 and Figure S3 of the SI, respectively) and regular horizontal interferometric color bands (Figure 6 and Figure S3 of the SI) with practically no stabilization associated with the disjoining pressure. Such horizontal uniformity of color bands was neither seen for the plane films of the superspreader SILWET L-77 (Figure 3, the inset images, and Figure 4) solutions, nor for the superspreader BREAK-THRU S 278 (Figure S2, the inset images, of the SI) solutions. Therefore, for the non-superspreaders the only parameter of interest to be elucidated from the present measurements is the surface elasticity ε, which is found from the measured values of the characteristic time T using the data in Figures 5 and S3 of the SI, similarly to ref 6. The results for the non-superspreader SILWET L-7607 solutions are summarized in Table 5, and for the non-superspreader BREAK-THRU S 233 in Table 6.

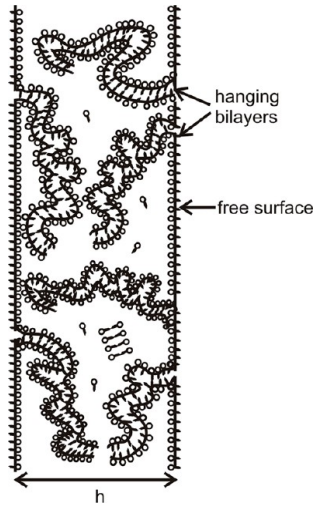

Figure 12. Sketch of fluffy surfaces of the film formed by long hanging superspreader bilayers.

Table 5. Non-superspreader SILWET L-7607 Solution Films[a]

solution	t (s)	t_b (s)	x (cm)	$h_i = h_0$ (nm)	T (s)	ε (g/s^2)
L-7607-0.1	5	4	0.1	201.45	4.8	0.013
L-7607-0.2	7	5	0.1	197.14	5.9	0.016
L-7607-0.5	10	8	0.1	199.62	8.7	0.024
L-7607-1.0	11	9	0.25	194.35	10.1	0.027

[a]The film lifetime is denoted t; t_b denotes the time at which black film sets in at the top of the wire frame. The x column corresponds to the position at the film center (reckoned from the top) to which the black film reached at the moment of bursting. The initial film thickness at the top is denoted $h_i = h_0$; the characteristic drainage time is T. The values of the surface elasticity ε were found from T using eq 17.

The difference between the superspreaders and the "cousin" non-superspreaders is only in the length of the poly(ethylene oxide) group. Yet, they show radically different drainage behavior, both morphologically and by duration. For example, the drainage of the superspreader SILWET L-77 and BREAK-THRU S 278 films is by an order of magnitude longer than the drainage of their non-superspreader counterparts SILWET L-7607 and BREAK-THRU S 233. The thinning of the superspreader films was practically arrested by the disjoining pressure at the latter stages of gravitational drainage, whereas the "cousin" non-superspreader

dx.doi.org/10.1021/la404754d | Langmuir XXXX, XXX, XXX−XXX

Table 6. Non-superspreader BREAK-THRU S 233 Solution Films[a]

solution	t (s)	t_b (s)	x (cm)	$h_i = h_0$ (nm)	T (s)	ε (g/s^2)
S 233-0.1	4	3.8	0.05	209.64	4.1	0.012
S 233-0.2	4	3.8	0.1	204.37	4.5	0.013
S 233-0.5	5	4.9	0.1	202.16	4.8	0.013
S 233-1.0	7	5	0.2	205.55	6	0.017

[a]The film lifetime is denoted t; t_b denotes the time at which black film sets in at the top of the wire frame. The x column corresponds to the position at the film center (reckoned from the top) to which the black film reached at the moment of bursting. The initial film thickness at the top is denoted $h_i = h_0$; the characteristic drainage time is T. The values of the surface elasticity ε were found from T using eq 17.

films drained without any visible inhibition and lasted for only a short time. Morphologically, the interferometric patters of the superspreader films during the drainage revealed a "turbulent"-like motion. On the contrary, the "cousin" non-superspreader films showed horizontal interference bands, indicating ordered drainage pattern characteristic of the ordinary surfactants (refs 6 and 26 and references therein).

CONCLUSIONS

Gravitational drainage of vertical films suspended on a rectangular wire frame is established as a relatively simple method of measurement of disjoining pressure. The effect of the disjoining pressure is in drastic deceleration of the later stage of the drainage process where the film thickness deviates (at about $h < 100$ nm) from the linear decrease sustained by the interplay of gravity and surface elasticity, and practically stabilizes at about ~35 nm. Gravitational drainage of two superspreaders SILWET L-77 and BREAK-THRU S 278 was dramatically stabilized in this manner, even though their interferometric patterns were highly dynamic and "turbulent"-like. The significant disjoining pressure revealed by the superspreaders is associated with the fluffy surfaces of the film formed by long superspreader bilayers hanging from the free surfaces (sketched in Figure 12). The ability to form long bilayer elements was attributed in the literature to the shorter length of poly(ethylene oxide) group in superspreaders compared to their non-superspreader "cousin" non-superspreaders SILWET L-7607 and BREAK-THRU S 233. The present work showed that these non-superspreaders do not possess any significant disjoining pressure in the ~35−100 nm range of the film thickness. Therefore, the non-superspreader gravitational drainage proceeds uninhibited, the thickness decrease is fully controlled by gravity and surface elasticity, and is not different from the ordinary surfactants. The scaling law for the disjoining pressure of the sufficiently concentrated superspreader solutions are $p_{disj}(h) \sim h^{-m}$ (with $m \approx 9-11$), as well as $p_{disj}(h) \sim h^{-s}$ (with $s \approx 6$) for more dilute solutions (in both cases concentrations were above the cmc). These scaling laws differ from those known for the entropic steric repulsions.

ASSOCIATED CONTENT

Supporting Information

The Supporting Information includes figures related to the surface tension measurements using the Wilhelmy plate technique, drainage of the superspreader BREAK-THRU S 278, and of the non-superspreader BREAK-THRU S 233, as well as videos of drainage processes corresponding to those in Figure 6. This information is available free of charge via the Internet at http://pubs.acs.org/.

AUTHOR INFORMATION

Corresponding Author

*To whom correspondence should be addressed. E-mail: ayarin@uic.edu. Phone: +1(312) 996-3472. Fax: +1(312) 413-0447.

Notes

The authors declare no competing financial interest.

ACKNOWLEDGMENTS

This work was partially supported by The U.S. Gypsum Corporation (USG).

REFERENCES

(1) Venzmer, J. Superspreading-20 years of physicochemical research. *Curr. Opin. Colloid Interface Sci.* **2011**, *16*, 335−343.
(2) Walderhaug, H.; Knudsen, K. D. Microstructures in aqueous solutions of a polyoxyethylene trisiloxane surfactant and a cosurfactant studied by SANS and NMR self-diffusion. *Langmuir* **2008**, *24*, 10637−10645.
(3) Venzmer, J. (personal communication).
(4) Karapetsas, G.; Craster, R. V.; Matar, O. On surfactant-enhanced spreading and superspreading of liquid drops on solid surfaces. *J. Fluid Mech.* **2011**, *670*, 5−37.
(5) Maldarelli, C. On the microhydrodynamics of superspreading. *J. Fluid Mech.* **2011**, *670*, 1−4.
(6) Sett, S.; Sinha-Ray, S.; Yarin, A. L. Gravitational drainage of foam films. *Langmuir* **2013**, *29*, 4934−4947.
(7) Derjaguin, B. V.; Churaev, V. N.; Muller, V. M. *Surface Forces*; Plenum Press: New York, 1987.
(8) Israelachvili, J. *Interfacial and Surface Forces*; Academic Press: London, 1992.
(9) Nikolov, A. D.; Kralchevsky, P. A.; Ivanov, I. B.; Wasan, D. T. Ordered micelle structuring in thin films formed from anionic surfactant solutions. *J. Colloid Interface Sci.* **1989**, *133*, 13−22.
(10) Basheva, E. S.; Kralchevsky, P. A.; Danov, K. D.; Ananthapadmanabhan, K. P.; Lips, A. The colloid structural forces as a tool for particle characterization and control of dispersion stability. *Phys. Chem. Chem. Phys.* **2007**, *9*, 5183−5198.
(11) Alexander, S. Adsorption of chain molecules with a polar head. A scaling description. *Physique* **1977**, *38*, 983−987.
(12) de Gennes, P. G. Polymers at an interface: A simplified view. *Adv. Colloid Interface Sci.* **1987**, *27*, 189−209.
(13) Scheludko, A. Thin liquid films. *Adv. Colloid Interface Sci.* **1967**, *4*, 391−464.
(14) Exerova, D.; Kruglyakov, P. M. *Foam and Foam Films. Theory, Experiment, Application*; Elsevier: Amsterdam, 1998.
(15) Mysels, K. J.; Jones, M. N. Direct measurement of the variation of double-layer repulsion with distance. *Discuss. Faraday Soc.* **1966**, *42*, 42−50.
(16) Karakashev, S. I.; Nguyen, A. V.; Manev, E. D.; Phan, C. M. Surface foam film waves studied with high-speed linescan camera. *Colloids Surf., A* **2005**, *262*, 23−32.
(17) Karakashev, S. I.; Nguyen, A. V. Do liquid films rupture due to the so-called hydrophobic force or migration of dissolved gases? *Langmuir* **2009**, *25*, 3363−3368.
(18) Karakashev, S. I.; Ivanova, D. S. Thin film drainage: Ionic vs. non-ionic surfactants. *J. Colloid Interface Sci.* **2010**, *343*, 584−593.
(19) Karakashev, S. I.; Stockelhuber, K. W.; Tsekov, R. Wetting films on chemically patterned surfaces. *J. Colloid Interface Sci.* **2011**, *363*, 663−667.
(20) Karakashev, S. I.; Manev, E. D.; Nguyen, A. V. Effect of double-layer repulsion on foam drainage. *Colloids Surf., A* **2008**, *319*, 34−42.
(21) Rao, A. A.; Wasan, D. T.; Manev, E. D. Foam stability − Effect of surfactant composition on the drainage of microscopic aqueous films. *Chem. Eng. Commun.* **1982**, *15*, 63−81.
(22) Danov, K. D.; Kralchevska, S. D.; Kralchevsky, P. A.; Ananthapadmanabhan, K. P.; Lips, A. Mixed solutions of anionic and

zwitterionic surfactant (Betaine): Surface-tension isotherms, adsorption, and relaxation kinetics. *Langmuir* **2004**, *20*, 5445−5453.
(23) *Phase Behavior of Surface-Active Solutes*. Particle Sciences, Drug Development Services, Technical Brief, 2012, Vol. *6*.
(24) Venzmer, J.; Wilkowski, S. P. Trisiloxane surfactants-Mechanisms of spreading and wetting. *ASTM Spec. Tech. Publ.* **1998**, *1347*, 140−154.
(25) Hill, R. M. *Silicone Surfactants*; Marcel Dekker: New York, 1999.
(26) Lucassen, J. Dynamic properties of free liquid films and foams. In *Anionic Surfactants. Physical Chemistry of Surfactant Action*; Lucassen-Reynders, E. H., Ed.; Marcel Dekker: New York, 1981; 217−265.
(27) Berg, S.; Adelizzi, E. A.; Troian, S. M. Experimental study of entrainment and drainage flows in microscale soap films. *Langmuir* **2005**, *21*, 3867−3876.
(28) Mysels, K. J. Dynamic processes in soap films. *J. Gen. Physiol.* **1968**, *52*, 113−124.
(29) Mysels, K. J.; Shinoda, K.; Frankel, S. *Soap Films. Studies of Their Thinning and a Bibliography*; Pergamon Press: London, 1959.
(30) Nierstrasz, V. A.; Frens, G. Marginal regeneration and the Marangoni effect. *J. Colloid Interface Sci.* **1999**, *215*, 28−35.
(31) Nierstrasz, V. A.; Frens, G. Marangoni flow driven instabilities and marginal regeneration. *J. Colloid Interface Sci.* **2001**, *234*, 162−167.
(32) Berg, S.; Adelizzi, E. A.; Troian, S. M. Images of the floating world: Patterns in thinning soap films. *Phys. Fluids* **2004**, *16*, S6.
(33) de Gennes, P. G. "Young" soap films. *Langmuir* **2001**, *17*, 2416−2419.
(34) Levich, V. G. *Physicochemical Hydrodynamics*; Prentice Hall: Englewood Cliffs, 1962.

dx.doi.org/10.1021/la404754d | *Langmuir* XXXX, XXX, XXX−XXX